The Journal of Global Radiology
ENSURING MEDICAL IMAGING ACCESS FOR ALL

PICTORIAL ESSAY

Imaging Spectrum of Skull Base Lesions: A Pictorial Essay

Rahul Ashokkumar (Rahul A.)[1]*, Yugandhar Samireddypalle[1], Arumulla Mithilesh[1], Prudhvinath Reddy Annapureddy[1], Mohammad Hafeezulla Shah[1], Manoj G. Kumar[1]

1. Department of Radiodiagnosis, All India Institute of Medical Sciences (AIIMS), Mangalagiri, Andhra Pradesh, India

* **Corresponding author.** Contact: rahulasok494@gmail.com

DOI: 10.7191/jgr.928

Published: 6/27/2025

Citation: Ashokkumar R, Samireddypalle Y, Mithilesh A, Annapureddy PR, Shah MH, Kumar MG. Imaging spectrum of skull base lesions: a pictorial essay. J Glob Radiol. 2025;11(2):928. Available from: https://doi.org/10.7191/jgr.928

Keywords: skull base, meningioma, cholesteatoma, schwannoma, aneurysm, chordoma

Word count: 1,637

Abstract

The skull base is a complex anatomical structure that supports the brain and contains multiple foramina, through which important structures such as the cranial nerves, spinal cord, and blood vessels pass. Various conditions can affect the skull base, such as infection, primary skull base tumors, invasion from head and neck malignancies, neural tumors, meningeal tumors, vascular pathologies, and developmental lesions. Diagnosis and management of these lesions require a multidisciplinary approach including neurosurgeons, otolaryngologists, and neuroradiologists. While both computed tomography (CT) and magnetic resonance imaging (MRI) are used in the characterization of these lesions, CT is better in the evaluation of bony changes and MRI is useful in evaluating surrounding soft tissue extension. This article depicts MRI and CT imaging appearances of a spectrum of skull base lesions.

Introduction

Different types of lesions can be seen in the skull base. Both computed tomography (CT) and magnetic resonance imaging (MRI) are used in the characterization of these lesions and for evaluation of their extent. MRI is helpful in soft tissue extension and CT is useful in the evaluation of bone erosions, bone expansion/sclerosis, and intratumoral calcification.

In this essay, we discuss some of the common skull base lesions and their imaging appearances.

Normal imaging of the skull base

The frontal, parietal, temporal, occipital, ethmoid and sphenoid bones form the calvarium and skull base. The calvarium is of predominant fat signal intensity on T1-weighted (T1W) and T2-weighted (T2W) images (1). T1W imaging can demonstrate the entire extent of the lesion due to the background bright fat signal, whereas T2W imaging along with T1W imaging can assess the tumor matrix characteristics.

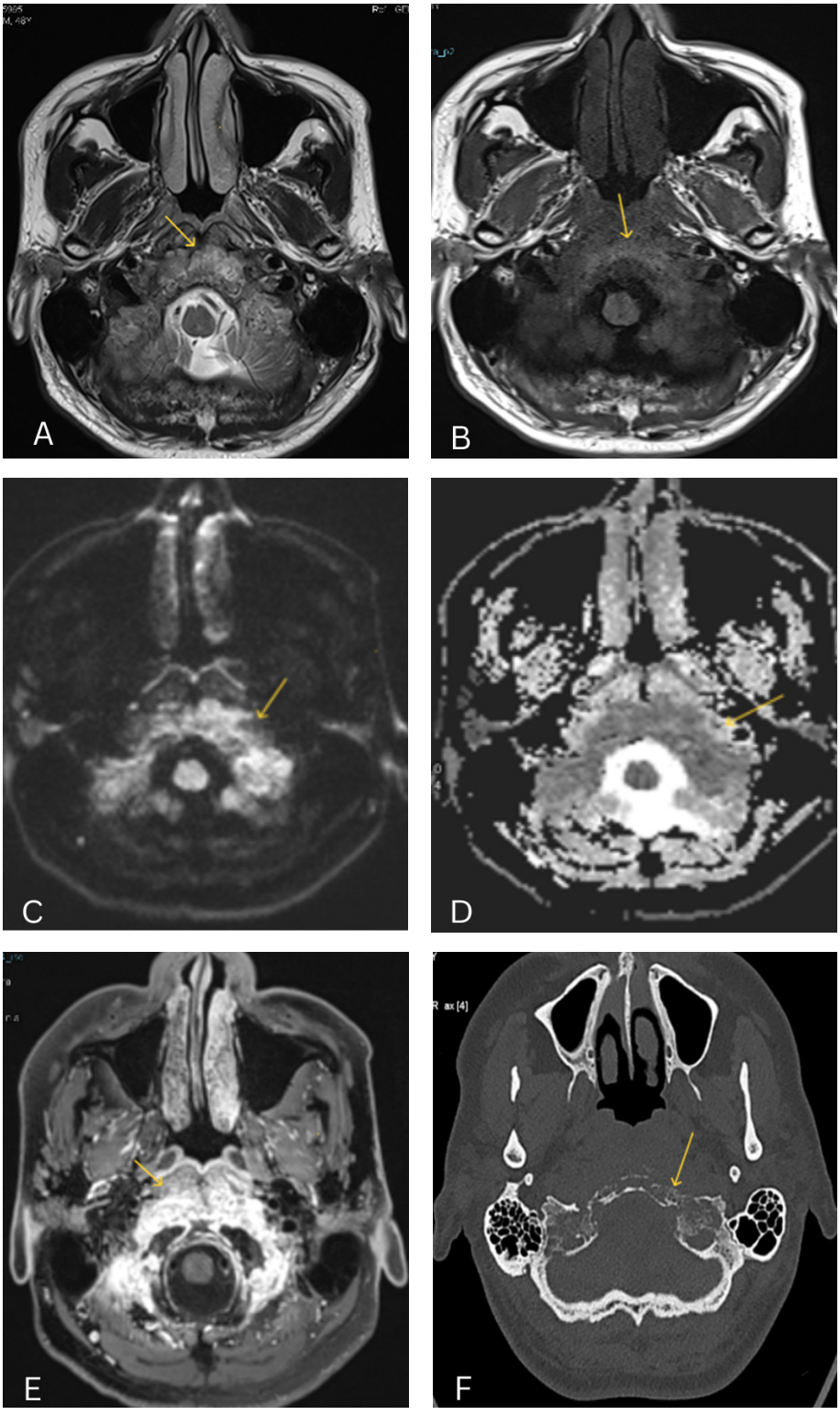

Infective lesions

Skull base osteomyelitis

Skull base osteomyelitis occurs as a contiguous spread from the adjacent infected structures, such as paranasal sinuses or middle ear/ mastoids (2).

Skull base osteomyelitis usually presents as altered areas of signal intensity replacing normal fatty marrow signal intensity on T1 and T2. Short tau inversion recovery (STIR) sequence highlights the surrounding soft tissue involvement (Figure 1). Contrast studies further determine the complete extent of the lesion in adjacent structures as well as intracranial/perineural extension (3).

Figure 1. Skull base osteomyelitis in a diabetic 62-year-old man presenting with vagal palsy (diagnosis is based only on imaging without histologic/ pathologic proof).

A, B. Diffuse altered signal intensity of the clivus and bilateral occipital condyles with associated T1 hypointensity and T2 heterogeneous hyperintense soft tissue.

C, D. Lesion demonstrating intense restricted diffusion. E. Intense heterogeneous enhancement on the post-contrast study with extension along bilateral jugular foramen.

F. Corresponding CT image demonstrating extensive destruction of involved bones (diagnosis is based only on imaging without histologic/pathologic proof).

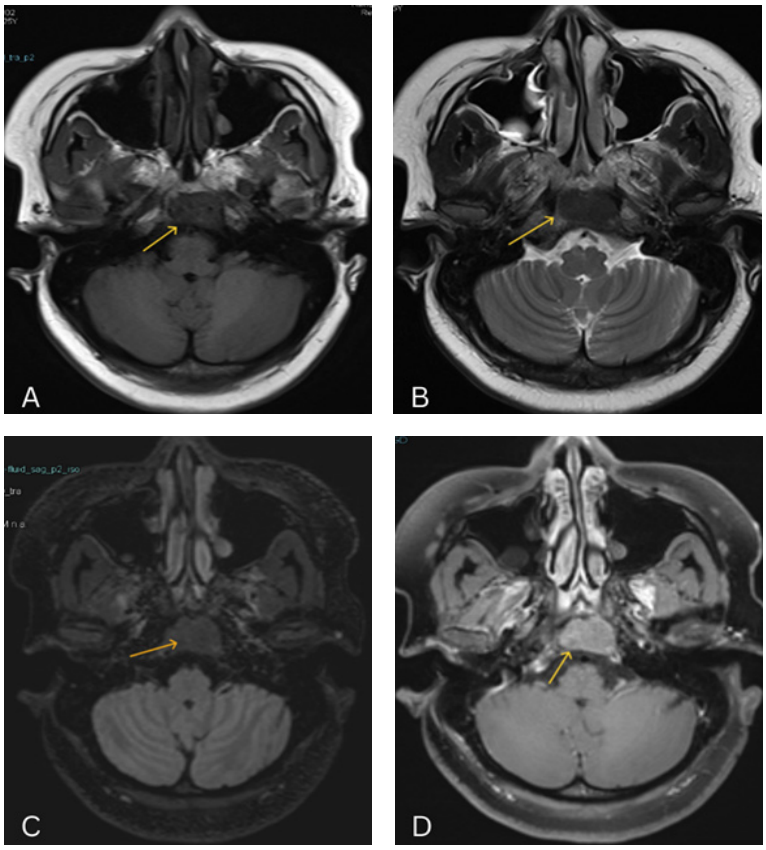

Primary skull base tumors

Giant cell tumor of the clivus

Giant cell tumor (GCT) of the clivus is very rare and can be completely benign, locally aggressive, or malignant with extension to the surrounding structures and cranial nerve involvement (4).

These lesions usually are isointense on T1 and hypointense on T2, and demonstrate variable restricted diffusion with homogeneous enhancement on contrast study (5) (Figure 2).

Figure 2. A 28-year-old woman on follow-up for presumptive diagnosis of GCT of the clivus (diagnosis is based only on imaging without histologic/pathologic proof).

A, B. Well circumscribed, smoothly marginated, T1 and T2 hypointense lesion within the clivus, with expansion of the marrow of the clivus and with thinning of anterior and posterior cortex and no cortical breach.

C. The lesion does not demonstrate restricted diffusion.

D. Moderate enhancement of the lesion in post-contrast study.

Chondrosarcoma

Chondrosarcoma is a malignant tumor arising from the chondroid cells. Approximately 1% of chondrosarcomas arise from the skull base, whereas most arise from the petroclival synchondrosis.

CT demonstrates the extent of the lesion and destruction of the skull base with multiple ring or half-ring calcifications (Figure 3). On MRI, the soft tissue extension of the lesion can be better delineated, and the lesion appears T1 hypointense and T2 hyperintense with variable degree of enhancement.

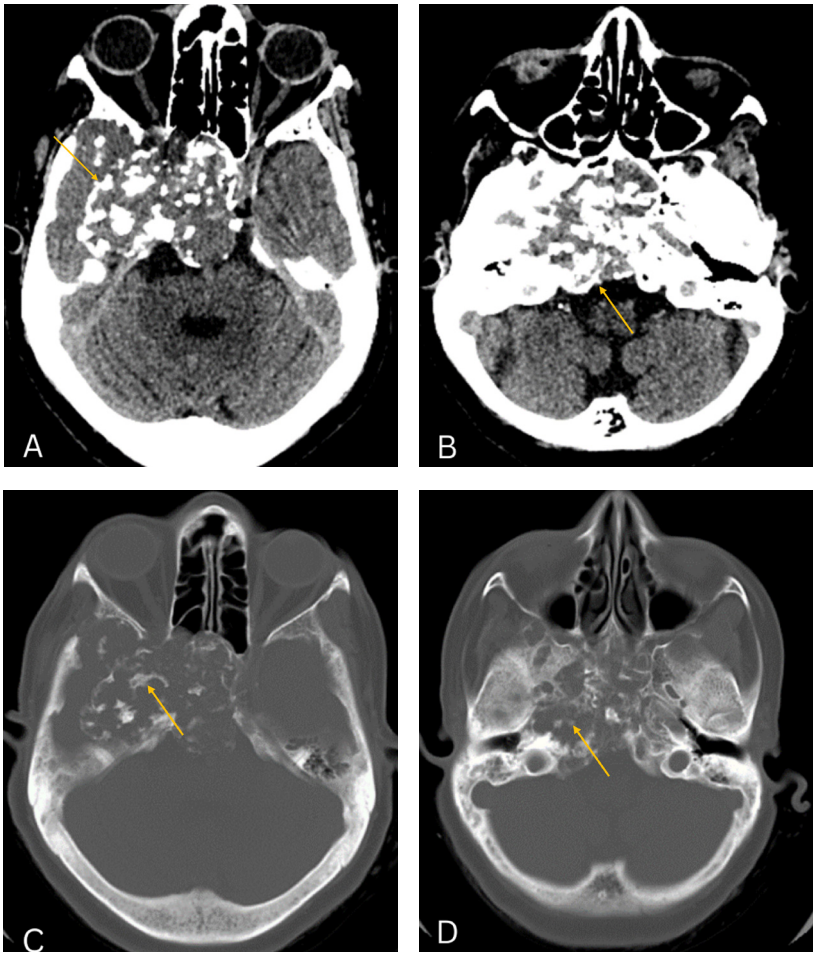

Figure 3. A 57-year-old woman on follow-up for HPE (histopathological examination) proven skull base chondrosarcoma.

A, B. A large, irregular expansile soft tissue density lesion with heterogeneous attenuation involving the clivus, sphenoid, right petrous apex and right greater wing of sphenoid (arrow).

C, D. CT bone window demonstrating extensive ring and half ring calcifications within the tumor matrix (arrow).

Chordoma

Chordomas are low-grade, locally aggressive tumors that arise from notochordal remnants (6). They most commonly occur along the axial skeleton. Approximately 35% arise at the skull base, particularly in the clivus. Other common sites include the spine and the sacrococcygeal region.

On MRI, the lesion usually appears to be T1 hypo to iso intense, T2 hyperintense with heterogeneous contrast enhancement (Figure 4). CT will help in the exact delineation of bony skull base destruction.

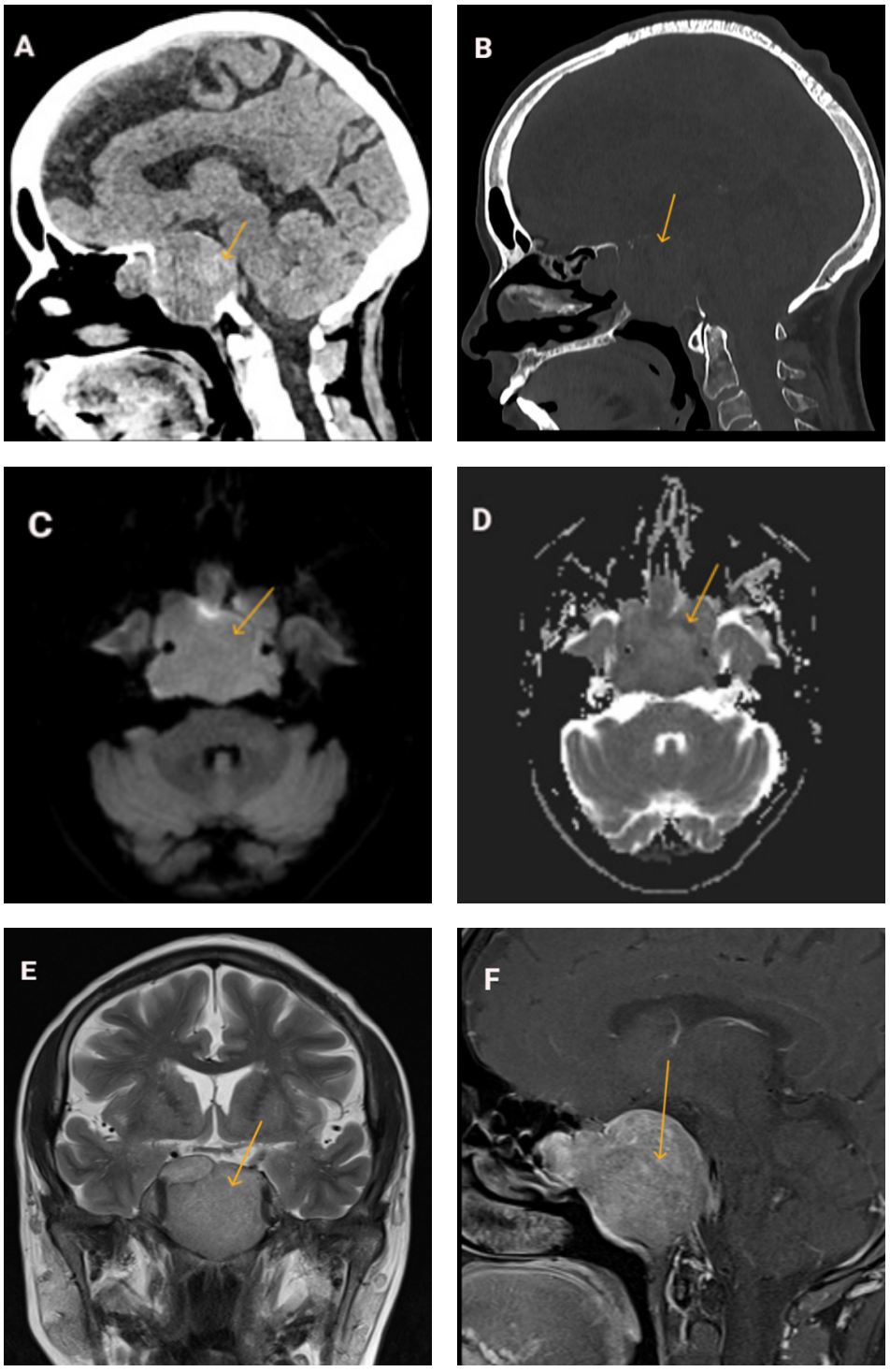

Figure 4. Clival chordoma (diagnosis based only on imaging without histologic/pathologic proof).

A. A large expansile heterogeneous soft tissue density lesion involving the clivus, sphenoid and the sella.

B. CT bone window demonstrating expansile lytic lesion with epicenter in the clivus.

C, D. Lesion demonstrates mild restricted diffusion.

E. Coronal T2W image demonstrating T2 hyperintense lesion encasing the cavernous parts of bilateral internal carotid arteries.

F. Post-contrast T1W image demonstrating heterogeneous enhancement of the lesion.

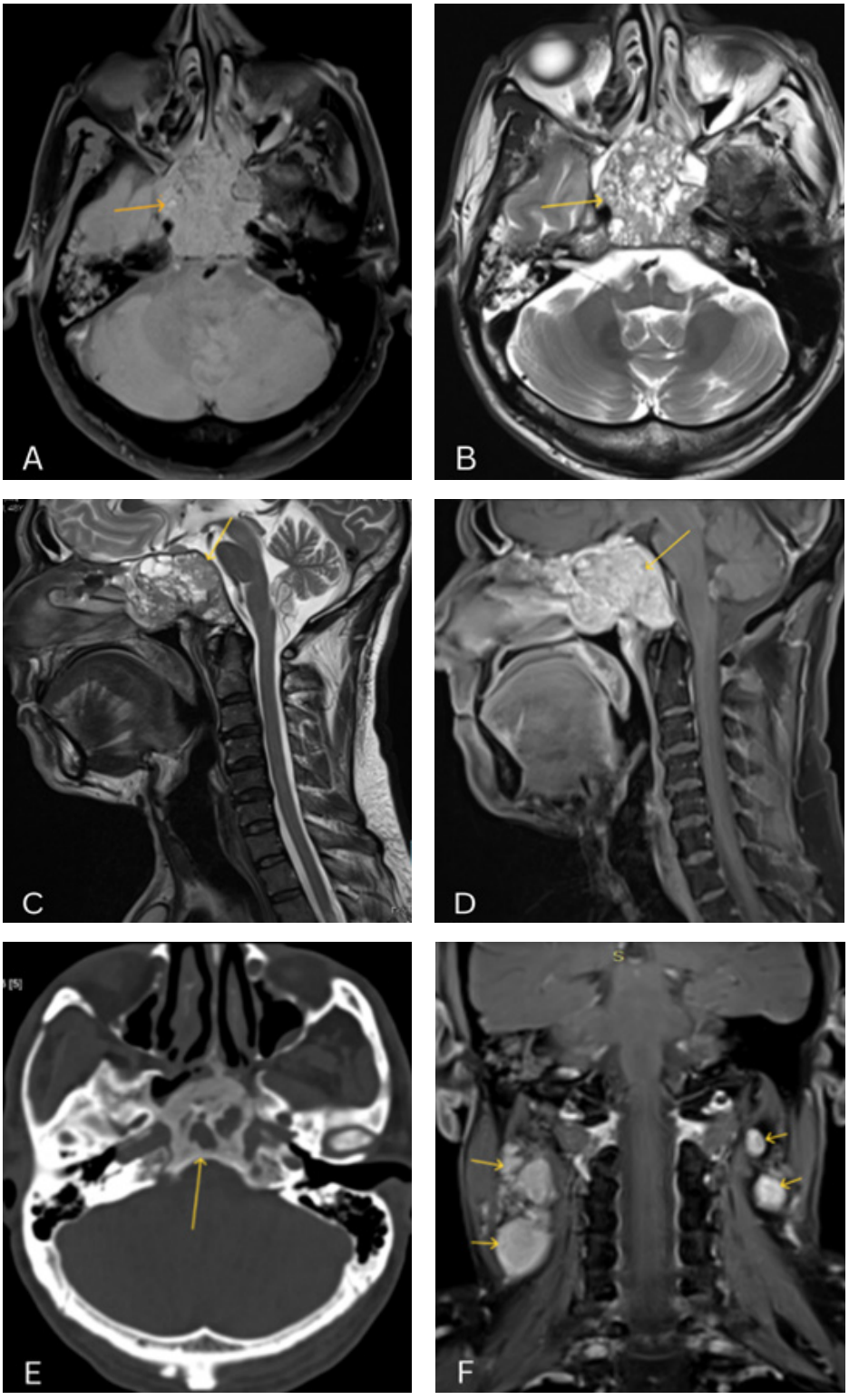

Skull base invasion from head and neck tumor

Nasopharyngeal carcinoma

The clivus and sphenoid bone are the most common sites affected by contiguous extension of the nasopharyngeal carcinoma (Figure 5) (7).

The lesion demonstrates heterogeneous signal intensity on T1 and T2. Contrast study gives proper delineation of the invasion of adjacent soft tissues, and perineural spread (8).

Figure 5. Contiguous extension of HPE (histopathological examination) proven nasopharyngeal carcinoma to the skull base.

A, B. Axial T1 and T2 W images demonstrating T1 hypointense and T2 heterogeneous hyperintense lesion completely replacing the clivus.

C, D. Sagittal T2 and post-contrast T1 W images demonstrating lesion epicenter in the roof and posterior wall of the nasopharynx.

E. CT scan at the corresponding level demonstrates mixed lytic and sclerotic areas within the clivus.

F. Metastatic bilateral cervical lymphadenopathy.

Invasive pituitary macroadenoma

Pituitary adenomas are classified as microadenomas if <10 mm and macroadenomas if >10 mm. On CT, there is expansion of the sella. However, in giant adenomas there can be erosion of the skull base.

On MRI, macroadenomas appear isointense with gray matter on T1W, T2W and show heterogeneous enhancement on T1 C+ (Figure 6). Microadenomas are inapparent on non- contrast images. As they enhance more slowly than normal pituitary tissue, they can be identified on dynamic contrast enhanced scans.

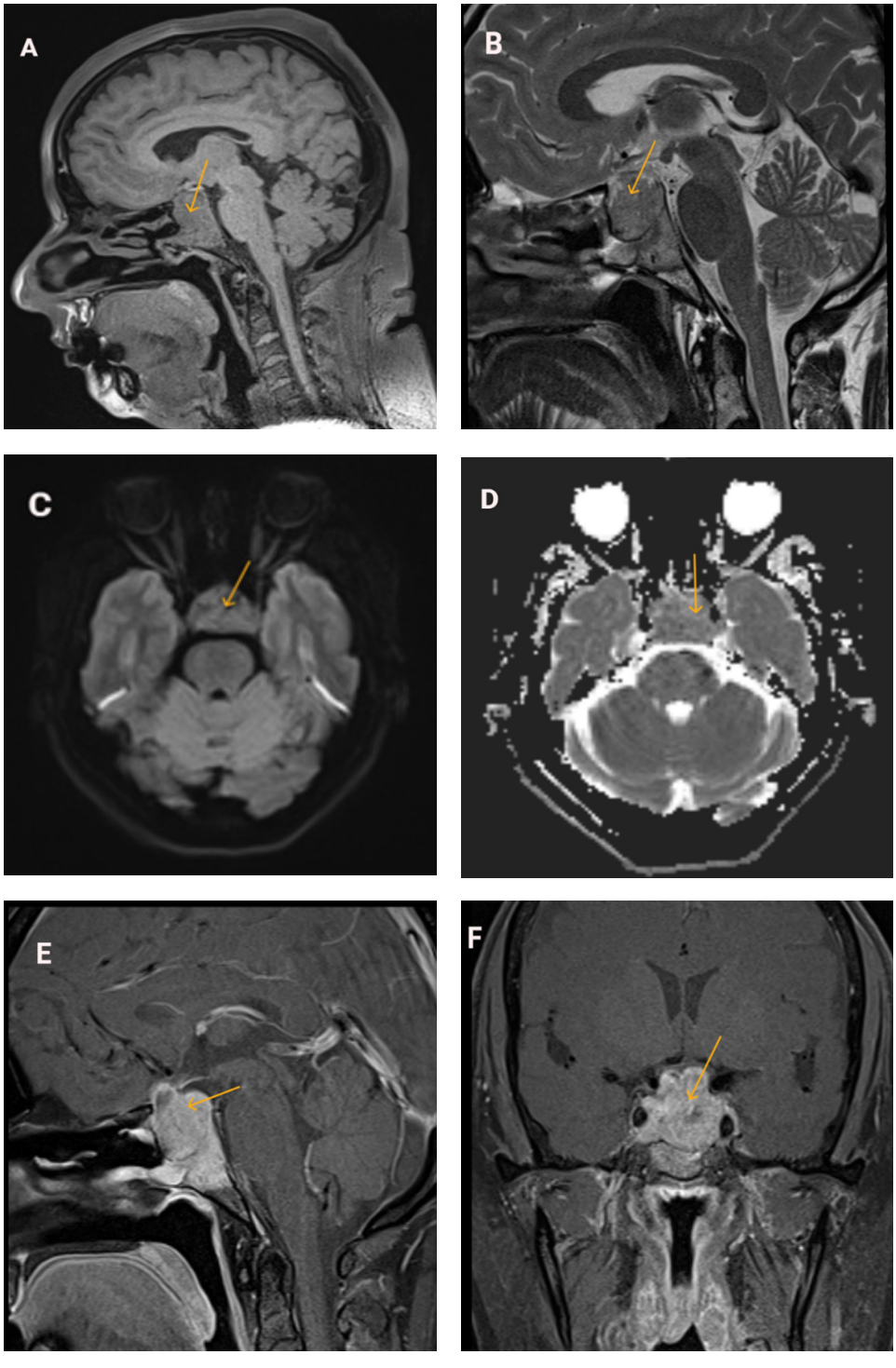

Figure 6. Recurrence of pituitary macroadenoma post-transsphenoidal resection in a 43-year-old woman, with invasion of the clivus.

A, B. A well-defined T1 isointense, T2 hyperintense lesion in the sella.

C, D. No significant restricted diffusion noted within the lesion.

E, F. Post-contrast T1W sagittal and coronal images demonstrating heterogeneously enhancing lesion invading the clivus, encasing the cavernous parts of left internal carotid artery with mild extension into the sphenoid sinus.

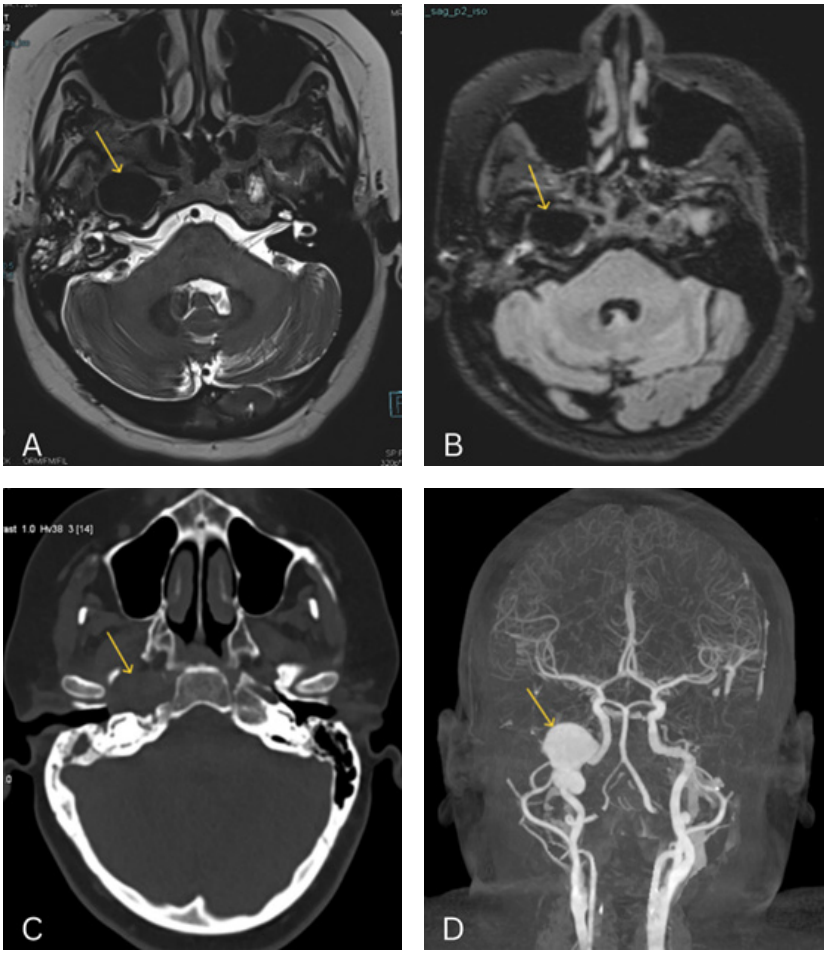

Vascular pathologies eroding the skull base

Although intracranial aneurysm rupture can cause significant morbidity and mortality, most unruptured skull base aneurysms are asymptomatic (9) (Figure 7).

The imaging appearances also can vary depending upon the wall thickness, presence or absence of eccentric mural thrombus, wall calcification, and luminal flow pattern (10). For these reasons, there may be absence of flow void and aneurysms may mimic tumors. CT angiography (CTA) or MR angiography (MRA) are required to evaluate the size and shape of an aneurysm and its origin.

Figure 7. Petrous ICA aneurysm in a middle-aged male with right ear pulsatile tinnitus.

A, B. Axial T2 and FLAIR images demonstrating a large flow void in the petrous canal of the right ICA, causing compression of the ipsilateral eustachian tube with right serous otitis media and mastoid effusion.

C. Axial CT bone window demonstrating expansion of the right petrous canal eroding the anterior wall of the right external auditory canal.

D. Coronal CT angiogram demonstrating bilobed saccular aneurysm of the right petrous ICA.

Developmental lesions

Fibrous dysplasia is a developmental bone disorder where normal bone is replaced by immature bone and fibrous tissue (11).

CT imaging findings demonstrate intramedullary expansile lesions demonstrating homogeneous ground glass densities. MRI signal intensity depends upon the histological pattern of the lesions (Figure 8) and can be variable low to intermediate signal intensity on both T1 and T2 W images with heterogeneous contrast enhancement (12).

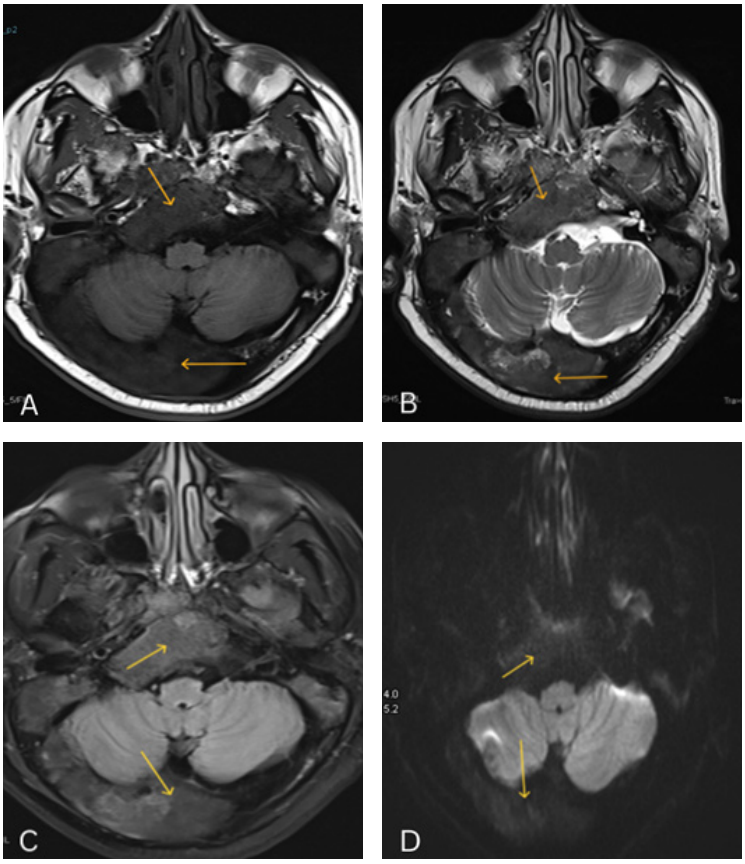

Figure 8. Fibrous dysplasia (diagnosis is based only on imaging without histologic/pathologic proof).

A, B. T1 and T2 hypointense islands of fibrous dysplasia involving the clivus and basiocciput are observed.

C. This island demonstrates heterogeneous FLAIR signal intensity.

D. No diffusion restriction noted in DWI.

Neural tumors

Schwannomas

Schwannomas are benign nerve sheath tumors, the majority of which arise from the eighth cranial nerve (Figure 9) (13).

These lesions are of low attenuation in CT and appear T1 hypointense and T2 hyperintense. On contrast administration, the majority of these lesions enhance intensely (14).

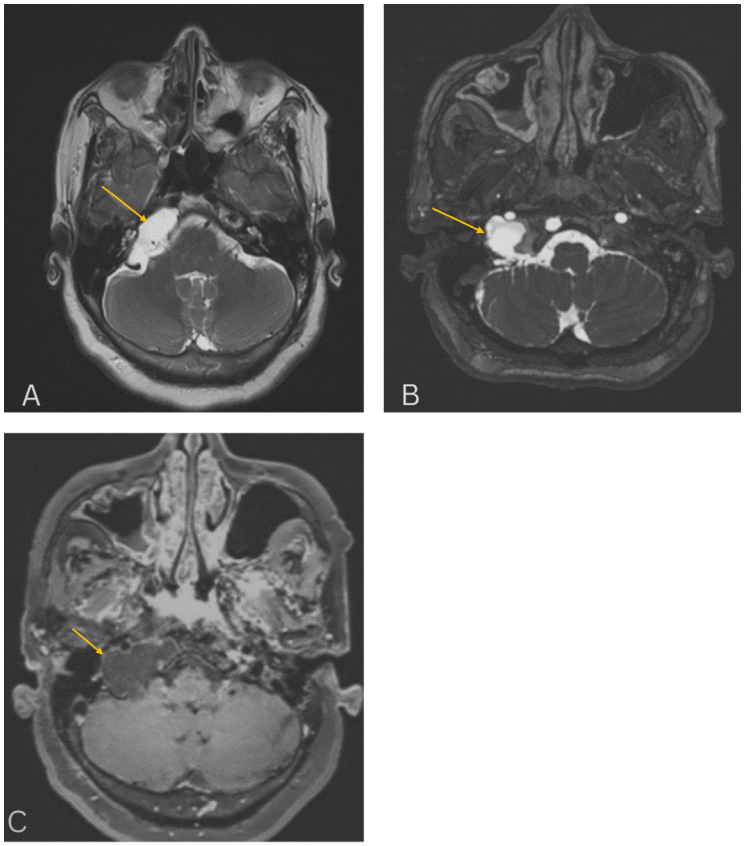

Figure 9. Jugular foramen Schwannoma (diagnosis is based only on imaging without histologic/pathologic proof).

A. Axial T2 W images at the level of the upper medulla demonstrate a well-defined T2 hyperintense lesion at the right petrous bone.

B. Axial CISS images confirm the lesion arising from the right jugular foramen.

C. Axial T1W post-contrast images reveal a thin peripheral rim of contrast enhancement.

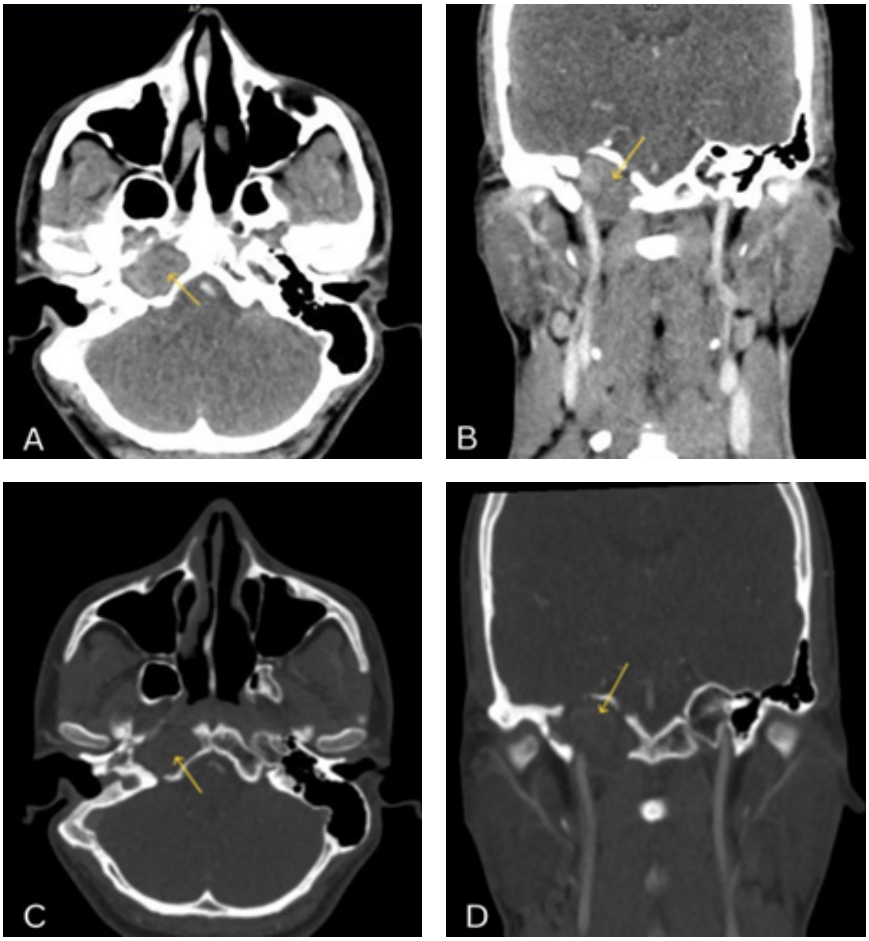

Miscellaneous

Cholesteatoma of petrous apex

Cholesteatoma of the petrous apex is a rare congenital condition (15).

CT scans are helpful to detect the presence of bone erosion (Figure 10). On MRI, imaging characteristics of congenital cholesteatomas are similar to those of epidermoid cysts, as they are histologically identical. They typically demonstrate hypointense signals on T1-weighted images, hyperintense signals on T2-weighted images and diffusion-weighted imaging (DWI), with corresponding low apparent diffusion coefficient (ADC) values.

Figure 10. Cholesteatoma of petrous apex (diagnosis is based only on imaging without histologic/pathologic proof).

A, B. Axial and coronal contrast-enhanced computed tomography (CECT) demonstrate a non-enhancing soft tissue density lesion at the apex of the right petrous bone.

C, D. Axial and coronal CT bone window demonstrates an expansile lytic lesion at the apex of the right petrous bone.

Conclusion

A large variety of lesions occur in the base of the skull. Some lesions appear in typical locations with typical imaging findings. CT and MRI are the main imaging modalities in detecting and characterizing these lesions. When vascular involvement is suspected, additional imaging, using methods such as CT angiography (CTA) or MR angiography (MRA), is essential for accurate assessment and preoperative planning. Understanding the pathology correlating with patient symptoms, and having knowledge of the spectrum of imaging findings, aid in the accurate diagnosis of these lesions.

References

1. Okada Y, Aoki S, Barkovich AJ, Nishimura K, Norman D, Kjos BO, et al. Cranial bone marrow in children: assessment of normal development with MR imaging. Radiol. 1989 Apr;171(1):161-4. Available from: https://doi.org/10.1148/radiology.171.1.2928520

2. Rothholtz VS, Lee AD, Shamloo B, Bazargan M, Pan D, Djalilian HR. Skull base osteomyelitis: the effect of comorbid disease on hospitalization. Laryngoscope. 2008 Nov;118(11):1917-24. Available from: https://doi.org/10.1097/MLG.0b013e31817fae0d

3. Álvarez Jáñez F, Barriga LQ, Iñigo TR, Roldán Lora F. Diagnosis of skull base osteomyelitis. Radiographics. 2021 Jan;41(1):156-74. Available from: https://doi.org/10.1148/rg.2021200046

4. Zhao J, Qian T, Zhi Z, Li Q, Kang L, Wang J, Sui A, Li N, Zhang H. Giant cell tumor of the clivus: A case report and review of the literature. Oncol Lett. 2014Dec ;8(6):2782-6. Available from: https://doi.org/10.3892/ol.2014.2528

5. Shibao S, Toda M, Yoshida K. Giant cell tumors of the clivus: case report and literature review. Surg Neurol Int. 2015 Nov;6(Suppl 25):S623. Available from: https://doi.org/10.4103/2152-7806.170459

6. Tenny S, Varacallo M. Chordoma StatPearls [Internet]. 2022 Feb 12. Available from: https://www.ncbi.nlm.nih.gov/books/NBK430846/

7. Li YZ, Cai PQ, Xie CM, Huang ZL, Zhang GY, Wu YP, Liu LZ, Lu CY, Zhong R, Wu PH. Nasopharyngeal cancer: impact of skull base invasion on patients prognosis and its potential implications on TNM staging. Eur J Radiol. 2013 Mar;82(3):e107-11. Available from: https://doi.org/10.1016/j.ejrad.2012.10.016

8. Razek AAKA, King A. MRI and CT of nasopharyngeal carcinoma. AJR Am J Roentgenol. 2012 Jan;198(1):11-8. Available from: https://doi.org/10.2214/AJR.11.6954

9. Chapman PR, Gaddamanugu S, Bag AK, Roth NT, Vattoth S. Vascular lesions of the central skull base region. In: Seminars in Ultrasound, CT and MRI. 2013 Oct (Vol. 34, No. 5, pp. 459-475). WB Saunders. Available from: https://doi.org/10.1053/j.sult.2013.09.003

10. Liu JK, Gottfried ON, Amini A, Couldwell WT. Aneurysms of the petrous internal carotid artery: anatomy, origins, and treatment. Neurosurg Focus. 2004;17(5):1-9. Available from: https://doi.org/10.3171/foc.2004.17.5.13

11. Chong VF, Khoo JB, Fan YF. Fibrous dysplasia involving the base of the skull. AJR Am J Roentgenol. 2002 Mar;178(3):717-20. Available from: https://doi.org/10.2214/ajr.178.3.1780717

12. Fitzpatrick KA, Taljanovic MS, Speer DP, Graham AR, Jacobson JA, Barnes GR, Hunter TB. Imaging findings of fibrous dysplasia with histopathologic and intraoperative correlation. AJR Am J Roentgenol. 2004 Jun;182(6):1389-98. Available from: https://doi.org/10.2214/ajr.182.6.1821389

13. Skolnik AD, Loevner LA, Sampathu DM, Newman JG, Lee JY, Bagley LJ, Learned KO. Cranial nerve schwannomas: diagnostic imaging approach. Radiographics. 2016 Sep;36(5):1463-77. Available from: https://doi.org/10.1148/rg.2016150199

14. Eldevik OP, Gabrielsen TO, Jacobsen EA. Imaging findings in schwannomas of the jugular foramen. AJNR Am J Neuroradiol. 2000 Jun;21(6):1139-44. Available from: https://pubmed.ncbi.nlm.nih.gov/10871029/

15. Gacek RR. Evaluation and management of primary petrous apex cholesteatoma. Otolaryngol Head Neck Surg1980 Sep-Oct;88(5):519-23. Available from: https://doi.org/10.1177/019459988008800502